

Rational Design of 2-Chloroadenine Derivatives as Highly Selective Phosphodiesterase 8A Inhibitors

Yadan Huang,[§] Xu-Nian Wu,[§] Qian Zhou,[§] Yinuo Wu, Dongxiao Zheng, Zhe Li, Lei Guo, and Hai-Bin Luo*Cite This: <https://dx.doi.org/10.1021/acs.jmedchem.0c01573>

Read Online

ACCESS |



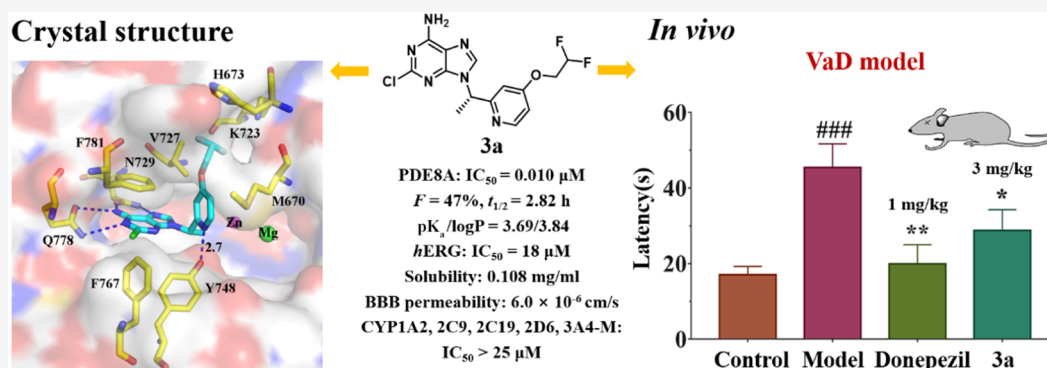
Metrics & More



Article Recommendations



Supporting Information



ABSTRACT: To validate the hypothesis that Tyr748 is a crucial residue to aid the discovery of highly selective phosphodiesterase 8A (PDE8A) inhibitors, we identified a series of 2-chloroadenine derivatives based on the hit clofarabine. Structure-based design targeting Tyr748 in PDE8 resulted in the lead compound **3a** (IC₅₀ = 0.010 μM) with high selectivity with a reasonable druglike profile. In the X-ray crystal structure, **3a** bound to PDE8A with a different mode from 3-isobutyl-1-methylxanthine (a pan-PDE inhibitor) and gave a H-bond of 2.7 Å with Tyr748, which possibly interprets the 220-fold selectivity of **3a** against PDE2A. Additionally, oral administration of compound **3a** achieved remarkable therapeutic effects against vascular dementia (VaD), indicating that PDE8 inhibitors could serve as potential anti-VaD agents.

INTRODUCTION

Both adenosine and guanosine 3',5'-cyclic monophosphate (cAMP and cGMP) serve as the momentous second messengers in intracellular signal transduction, and their signaling systems are involved in the regulation of a series of physiological processes, including learning and memory, cell differentiation and proliferation, immune/inflammatory responses, airway smooth muscle relaxation, visual signal transduction, and metabolic functions.^{1–3} As the only enzymes to degrade cAMP and cGMP, phosphodiesterases (PDEs) are important drug targets for a variety of diseases,^{4–7} and over 20 marketed inhibitors^{1–8} have been approved including selective PDE4/5 inhibitors, such as apremilast, sildenafil, and tadalafil, and nonspecific PDE inhibitors, such as theophylline, pentoxifylline, and dipyridamole. These selective PDE4/5 inhibitors are used in clinics against psoriasis, erectile functions, and pulmonary hypertension.^{4,5,8}

Among the three cAMP-specific PDE isoforms (PDE4, 7, and 8),⁸ PDE4 is arguably the most studied of all PDE families, and several studies suggested that PDE4 inhibition could be used to treat cognitive dysfunctions^{9–12} and memory impairment.^{13,14} Additionally, our recent studies demonstrated that

PDE4 inhibitors could be used to prevent vascular dementia (VaD).¹⁵ Many studies suggest that increasing cAMP signaling in a brain region-specific manner may prove a viable mechanism for treating age-related decline in brain functions.^{16–19} However, most PDE4 inhibitors show severe side effects, such as vomiting, diarrhea, and weight loss.^{9–12} Relative to PDE4 (K_m of 1–10 μM for cAMP),^{4,20} PDE8 has a stronger affinity for cAMP (K_m of 40–150 nM for cAMP).^{21–23} Therefore, we speculate that PDE8 is similar to PDE4 as a drug target for nervous system diseases and its inhibitors have potential therapeutic effects on cognitive dysfunctions such as VaD,¹⁵ which is a very common subtype of dementias.²⁴

However, few studies have attempted to identify selective phosphodiesterase 8A (PDE8A) inhibitors, which could be

Received: September 8, 2020



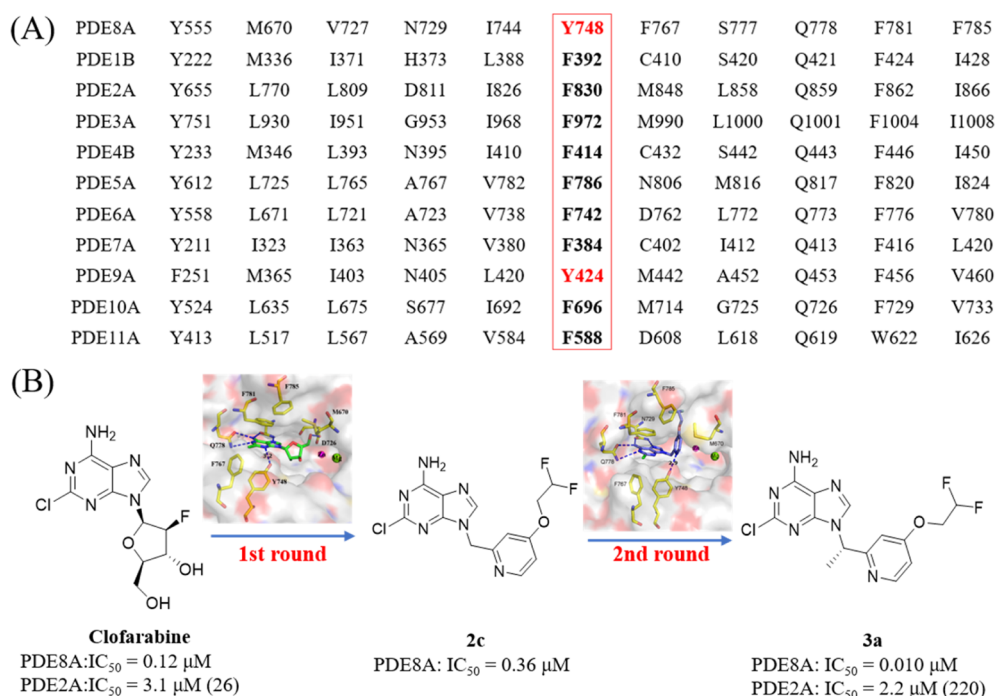


Figure 1. Structure-based optimizations of 2-chloroadenine derivatives as novel PDE8A inhibitors with improved potency and selectivity by targeting Tyr748. (A) Sequence alignment of the residues in the active site across PDE families. (B) Two rounds of structural optimizations based on clofarabine resulted in the highly potent PDE8A inhibitor 3a. The PDB IDs are 7CWA and 7CWF for the crystal structures of the PDE8A–clofarabine and PDE8A–2c complexes (see their binding patterns in high resolution in Figure 2), respectively.

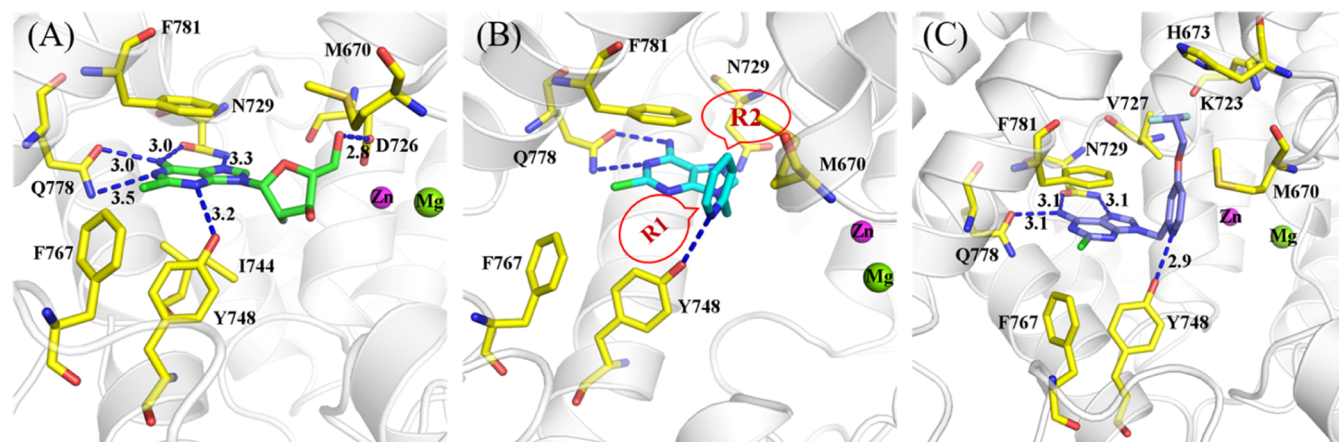


Figure 2. Structure-based optimization of selective PDE8A inhibitors. (A) Cartoon presentation of clofarabine binding to the active pocket of PDE8A (green sticks, PDB ID: 7CWA). (B) Design of a scaffold that may potentially form a H-bond with Tyr748 and fit tightly to the PDE8A pocket. (C) Cartoon presentation of 2c binding to the pocket of PDE8A (purple sticks, PDB ID: 7CWF).

used as chemical probes to explore the biological functions of PDE8.^{25–27} PDE8 and PDE9 have the lowest K_m values among cAMP-specific and cGMP-specific PDE families, respectively,^{4,23,28} and share the same/unique residue (Tyr748 in PDE8, Tyr424 in PDE9, Figure 1A) in the PDE superfamily. Our previous studies resulted in two highly selective PDE9 inhibitors (28 and 3r, Figure S1) with a common scaffold of pyrazolo[3,4-*d*]pyrimidinone by targeting the unique tyrosine residue Tyr424.^{29,30} Thus, we speculate that the unique residue Tyr748 is an important residue in PDE8A that can promote the discovery of highly selective PDE8A inhibitors.

In our previous study, clofarabine exhibited an IC₅₀ of 3.1 μM toward PDE2A.³¹ Herein, we identified clofarabine with an IC₅₀ of 0.12 μM against PDE8A, which gave a poor selectivity

of 26-fold against PDE2A. To validate the hypothesis that Tyr748 is a crucial residue to aid the discovery of highly selective PDE8A inhibitors, medicinal chemistry optimizations targeting Tyr748 (Figures 1 and 2) were performed based on the hit clofarabine. As a result, lead 3a (IC₅₀ = 0.010 μM) gave high selectivity and a reasonable druglike profile. Notably, the X-ray crystal structure of the PDE8A–3a complex first showed the binding pattern between a selective inhibitor and PDE8A, which could aid in the discovery of novel PDE8A inhibitors. In addition, oral administration of 3a could achieve spatial learning and memory improvement in the VaD mice model, indicating that PDE8 inhibitors could serve as potential agents against VaD.

RESULTS AND DISCUSSION

Our previous research revealed that clofarabine showed moderate inhibition against PDE2 ($IC_{50} = 3.1 \mu M$).³¹ Herein, a screening of the FDA drug database was performed to identify potent PDE8A inhibitors, and clofarabine was identified as a hit with an IC_{50} of $0.12 \mu M$ against PDE8A (Figure S2).

To understand the binding pattern between clofarabine and PDE8A, we obtained the crystal structure of the PDE8A–clofarabine complex. In Figure 2A, the 2-chloroadenine core of clofarabine served as the scaffold that is sandwiched in the hydrophobic clamp between Phe781 and Ile744/Tyr748, and it provides four H-bonds with Gln778 and Asn729. The ribose moiety of clofarabine stretches toward the metal binding pocket, and it forms a H-bond with Asp726. These interactions together contributed to the inhibitory potency. Additionally, clofarabine forms a relatively weak H-bond with Tyr748 (3.2 \AA) that is unique to PDE8A, which may account for its relatively poor selectivity.

Rational Design of Highly Selective PDE8A Inhibitors Targeting Tyr748. The hit-to-lead optimizations were performed based on clofarabine in order to improve potent inhibition against PDE8A as well as improve selectivity over PDE2 and other PDEs. According to sequence alignment of the residues in the active site (Figure 1A), PDE8A as well as PDE9A contains a tyrosine residue at position 748, while the others contain phenylalanine. Therefore, introducing a H-bond with PDE8A Tyr748 may provide a new avenue for selectivity over other PDEs. To validate this strategy, we designed a pyridin-2-yl methyl group to replace the ribose moiety to improve the H-bond interaction between the N atom of pyridine and the hydroxyl group of Tyr748 (Figure 2B). Based on the molecular docking studies, the ortho position of pyridine is suitable to introduce substituents with a large space volume (R_1 groups, Table 1 and Scheme 1) to fit the solvent-filled side pocket, while the para position is suitable to introduce relatively small substituents (R_2 groups, Table 1 and Scheme 2) to occupy a hydrophobic subpocket (Figure 2B).

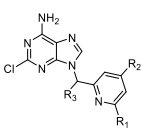
Therefore, we first designed and synthesized compounds 1a–i and 2a–c. Compound 1g (R_1 was the cyclopentyl group) showed a 1.6-fold higher inhibitory activity than clofarabine (0.046 vs $0.12 \mu M$). However, 1c–f, 1h–i, and 2a–c only showed moderate inhibitory activities against PDE8A (IC_{50} , 0.13 – $0.92 \mu M$), and 1a–b showed weak inhibitory activities ($IC_{50} > 1 \mu M$). Interestingly, the cocrystal structure of PDE8A with bound 2c ($IC_{50} = 0.36 \mu M$) was achieved. As shown in Figure 2C, 2c with a difluoroethoxyl substitution at the para position of pyridine occupies the same pocket as clofarabine. The interaction between 2c and Tyr748 is reinforced from 3.2 to 2.9 \AA compared with the PDE8A–clofarabine complex.

To improve the inhibitory potency of 2c, a methyl group (R_3) was introduced to restrict the rotational freedom of the pyridin-2-yl methyl group, generating 3, 3a, and 3b. As a result, inhibitor 3a with an IC_{50} value of $0.010 \mu M$ was discovered (Scheme 3 and Table 1).

To remove the pan-assay interference compounds (PAINS), we performed a virtual screening of the designed 15 compounds by the online program “PAINS-Remover”,³² and all the compounds passed the filter (<http://www.cbligand.org/PAINS/>).

Chemistry. The synthetic routes for the 2-chloroadenine derivatives are depicted in Schemes 1–3. For the preparation

Table 1. Inhibitory Affinities (IC_{50}) of Targeted Compounds against PDE8A



Compd.	R_1	R_2	R_3	IC_{50} (μM) ^a
1a	H	H	H	24% ^b
1b	–CH ₃	H	H	14% ^b
1c		H	H	0.27 ± 0.03
1d		H	H	0.13 ± 0.01
1e		H	H	0.25 ± 0.01
1f		H	H	0.25 ± 0.03
1g		H	H	0.046 ± 0.002
1h		H	H	0.22 ± 0.01
1i		H	H	0.92 ± 0.02
2a	H	Cl	H	0.41 ± 0.04
2b	H	–OCH ₃	H	0.66 ± 0.05
2c	H		H	0.36 ± 0.01
3	H		–CH ₃	0.026 ± 0.004
3a/(S)-3	H		(S)–CH ₃	0.010 ± 0.001
3b/(R)-3	H		(R)–CH ₃	2.8 ± 0.1

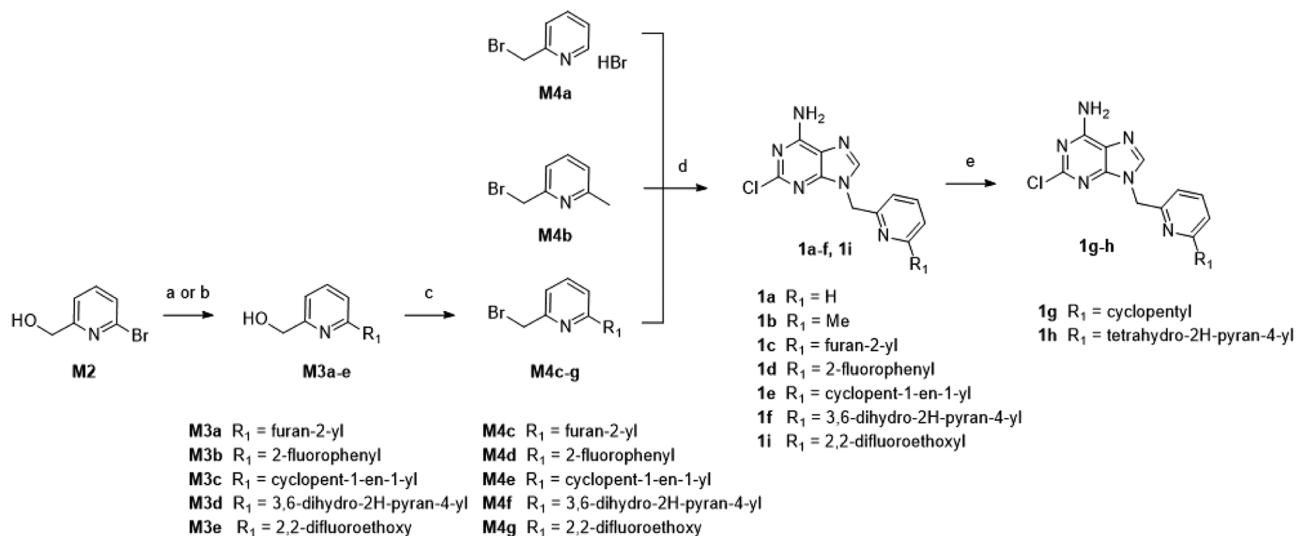
^a Values are given as the mean \pm SD of three different experiments.

^b Inhibitory ratio at concentration $1 \mu M$.

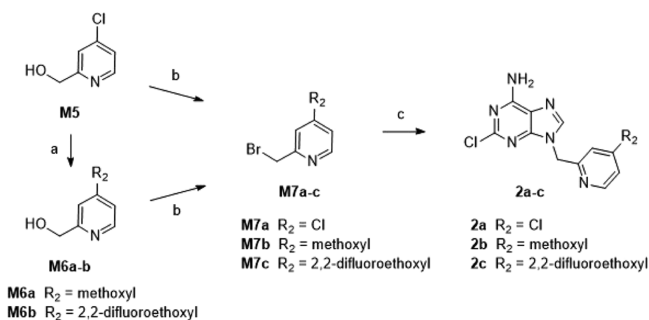
of the target compounds 1a–i (Scheme 1), intermediates M3a–e were synthesized by Suzuki coupling³³ between boronic ester M1 and aryl bromide M2 or substitution with sodium alcoholate. Then, the bromination of M3a–e with PBr₃ gave the key intermediates M4c–g. The commercial intermediates M4a–b and the key intermediates M4c–g reacted with 2-chloro-9H-purin-6-amine using Cs₂CO₃ as the base, yielding compounds 1a–f and 1i. Compounds 1e and 1f were reduced by Pd–C/H₂ to produce 1g and 1h.

The synthetic routes for the preparation of compounds 2a–c are shown in Scheme 2, which is similar to Scheme 1 for the synthesis of compounds 1a–i. M5 was substituted with sodium alcoholate, followed by bromination with PBr₃ to yield the key intermediates M7a–c. Then, M7a–c were treated with 2-chloro-9H-purin-6-amine in the presence of Cs₂CO₃ to obtain compounds 2a–c.

As shown in Scheme 3, the key intermediate M12 was synthesized by substitution with sodium alcoholate, Suzuki coupling³³ with pinacol vinylboronate, reduction with Pd–C/H₂, and Wohl–Ziegler bromination^{34,35} with N-bromosuccinimide (NBS). Then, reaction of M12 with 2-chloro-9H-purin-6-amine in the presence of Cs₂CO₃ led to compound 3.

Scheme 1. Synthetic Route for Compounds 1a–i^a

^aReagents and conditions: (a) boric ester or boric acid derivatives (**M1**), Pd(dppf)Cl₂·CH₂Cl₂, K₂CO₃, 1,4-dioxane/H₂O, 100 °C, overnight; (b) sodium 2,2-difluoroethanolate, 2,2-difluoroethanol, reflux, 16 h; (c) PBr₃, DCM, 0 °C to r.t., 4 h; (d) 2-chloro-9H-purin-6-amine, Cs₂CO₃, DMF, 70 °C, overnight; (e) Pd/C, H₂, MeOH/THF, r.t., overnight.

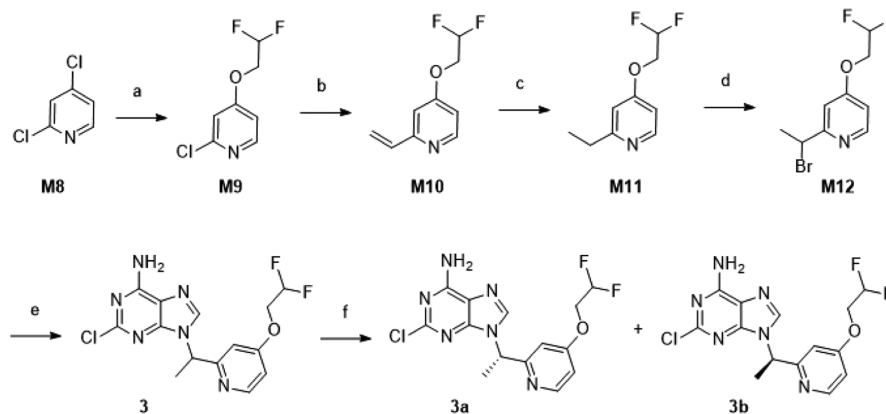
Scheme 2. Synthetic Route for Compounds 2a–c^a

^aReagents and conditions: (a) sodium methoxide or sodium 2,2-difluoroethanolate, MeOH or 2,2-difluoroethanol, reflux, 16 h; (b) PBr₃, DCM, 0 °C to r.t., 4 h; (c) 2-chloro-9H-purin-6-amine, Cs₂CO₃, DMF, 70 °C, overnight.

Racemate **3** was separated to both the (*R*)-isomer and (*S*)-isomer using a CHIRALFLASH IA column.

Structure–Activity Relationships. We determined the inhibitory potencies of the compounds against PDE8A in Table 1, and the IC₅₀ values with standard deviation (SD) data are listed in Table 1.

For compounds **1a–i**, different R₁ groups were introduced at the ortho position of the pyridine ring. When R₁ was a hydrogen atom (**1a**) or methyl group (**1b**), the compound exhibited weak inhibitory activity with an IC₅₀ value greater than 1 μM, indicating that an R₁ group with a small volume may not be suitable. Compounds **1c–i**, with larger volumes of R₁ groups, exhibited significant enhancement of the inhibitory potency against PDE8A. Among the ortho position-substituted compounds (**1a–i**), cyclopentyl-substituted compound **1g** (IC₅₀ = 0.046 μM) exhibited better inhibitory activity than other compounds.

Scheme 3. Synthetic Route for Compounds 3, 3a, and 3b^a

^aReagents and conditions: (a) sodium 2,2-difluoroethanolate, 2,2-difluoroethanol, reflux, 16 h; (b) pinacol vinylboronate, Pd(dppf)Cl₂·CH₂Cl₂, K₂CO₃, 1,4-dioxane/H₂O, 100 °C, overnight; (c) Pd/C, H₂, MeOH/THF, r.t., overnight; (d) NBS, AIBN, CCl₄, reflux, 4 h; (e) 2-chloro-9H-purin-6-amine, Cs₂CO₃, DMF, 70 °C, overnight; (f) chiral separation, CHIRALFLASH IA column, DCM/THF 99:1, 12 mL/min.

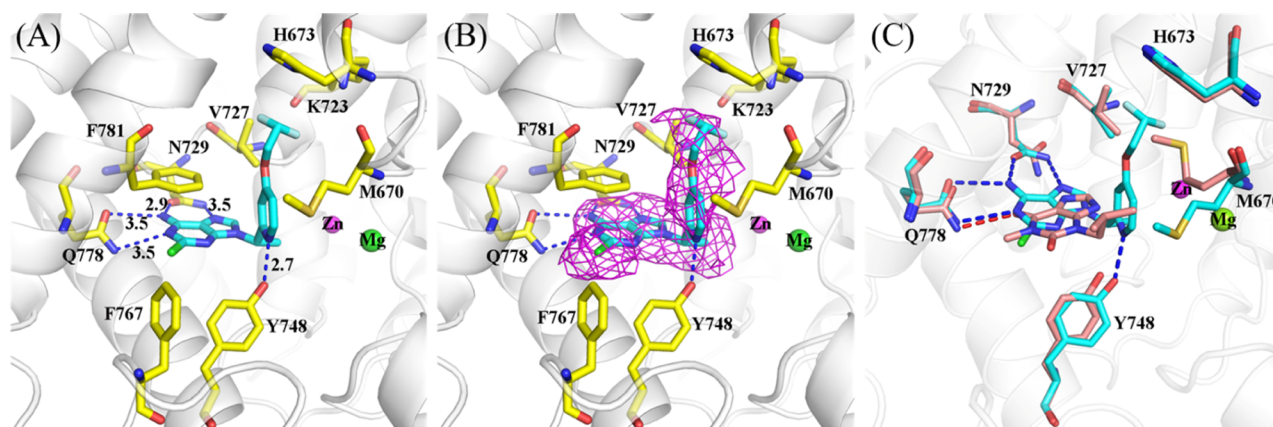


Figure 3. Cocystal structures of the PDE8A–3a complex. (A) Cartoon model for PDE8A in complex with 3a (cyan sticks, PDB ID: 7CWG); the dotted lines represent H-bonds. (B) Electron density maps of (Fo–Fc) for PDE8A in complex with 3a (cyan sticks). (C) Differences in the binding patterns between PDE8A–3a (cyan sticks) and PDE8A–IBMX (pink sticks, PDB ID: 3ECN).

For compounds **2a–c**, different R_2 groups were introduced at the para position of the pyridine ring. Compared to compound **1a** with no substituent on the R_2 position, the inhibitory activities of all these three compounds were improved. Compound **2a** ($R_1 = \text{Cl}$) showed moderate inhibitory activity against PDE8A ($\text{IC}_{50} = 0.41 \mu\text{M}$). A methoxyl group and 2,2-difluoroethoxy group were introduced on the para position to form compounds **2b** and **2c**. The inhibitory activity order of the substituents from high to low is $-\text{OCH}_2\text{CHF}_2 > -\text{OCH}_3$, implying that a certain length of R_2 group is favorable for the binding. Compared with compound **1i** with $-\text{OCH}_2\text{CHF}_2$ at the ortho position, compound **2c** exhibited about 1.6-fold higher inhibitory activity than **1i** (0.36 vs $0.92 \mu\text{M}$), implying that the substitution of $-\text{OCH}_2\text{CHF}_2$ at the para position of pyridine is more beneficial to the inhibitory activity than that at the ortho position.

Based on the binding pattern of **2c**, we considered that the restriction of the active conformation is beneficial to inhibitory activity, and a methyl group was introduced to restrict the rotational freedom of the pyridin-2-yl methyl group of **2c** to obtain **3**. Notably, **3** showed approximately 13-fold higher inhibition than **2c** (0.026 vs $0.36 \mu\text{M}$). We also obtained the two enantiomers of compound **3** (**3a** and **3b**), confirming that the (*S*)-isomer (**3a**) gave a better IC_{50} value of $0.010 \mu\text{M}$ against PDE8A than **3b**. This improvement in affinity appears to be mainly due to the introduction of another methyl moiety at the R_3 position. In Table 1, **3a** gave an IC_{50} of $0.010 \mu\text{M}$, similar to that ($0.026 \mu\text{M}$) of its racemic form **3**, while **3b** had an IC_{50} of $2.8 \mu\text{M}$, which suggested that the (*S*)-isomer significantly enhanced its inhibition with PDE8 compared to the (*R*)-isomer. In view of the more potent affinity against PDE8A, **3a** was used in the subsequent studies.

Validation of the Key Tyr748 via the Cocystal Structure. In Figure 3, the binding pattern of PDE8A with **3a** was revealed by the electron density maps of (Fo–Fc) of the X-ray crystal structure. It is clear that the adenine ring of **3a** is clamped tightly in the bay surrounded by Asn729, Gln778, and Phe781 because the amine of the adenine ring forms two H-bonds with the amide oxygen of the Gln778 side chain (3.5 \AA) and Asn729 side chain (2.9 \AA). Besides the π – π interactions with residues Phe781, the adenine ring of **3a** also forms a H-bond with the amide nitrogen of Gln778/Asn729 (3.5 \AA to both nitrogens). Importantly, the pyridine ring forms a stronger H-bond of 2.7 \AA with the hydroxyl group

of Tyr748, which may account for the improvement of the selectivity index against PDE2A from 26-fold for clofarabine to 220-fold and validated that Tyr748 is a crucial residue for the discovery of potent PDE8A inhibitors.

Different Binding Patterns of 3a from 3-Isobutyl-1-methylxanthine. In Figure 3C, the planar xanthine core of 3-isobutyl-1-methylxanthine (IBMX) forms π – π stacking with the benzene ring of Phe781, and the carbonyl oxygen forms a weak H-bond with the N atom of the Gln778 amide group at a distance of 3.4 \AA , which is the only H-bond detected (PDB ID: 3ECN).³⁶ Unlike IBMX, **3a** shows much stronger interactions with three residues (Tyr748, Asn729, and Gln778) to form five H-bonds mentioned above as shown in Figure 3A. Among these, two H-bonds between **3a** and Asn729 are formed because the side chain undergoes the structural transformation with a Chi angle of 50.19° changed from -57.43° in the PDE8A–IBMX complex. It is noted that the pyridine of **3a** involved a strong H-bond of 2.7 \AA with Tyr748, resulting in high selectivity over other PDEs, which is not observed in the crystal structure of PDE8A with bound IBMX. Additionally, the difluoroethoxyl side chain of **3a** induced a conformational change in Met670 (Figure 3C).

Remarkable Selectivity Profile of Compound 3a. The selectivity profile (Table 2) of compound **3a** across PDE isoforms was determined. Its inhibitory affinities (IC_{50}) against PDE1B, PDE3A, PDE5A1, PDE7A1, PDE9A2, and PDE11A4 were no less than $10 \mu\text{M}$, and the IC_{50} values against PDE2A, PDE4D2, and PDE10A were 220-fold, 710-fold, and 440-fold higher than those against PDE8A1, respectively. In short, the

Table 2. Selectivity Profile of **3a** across PDE Families

PDEs	IC_{50} (μM)	selectivity (fold)
PDE8A1 (480–820)	0.010 ± 0.001	
PDE1B (146–506)	>10	>1000
PDE2A (580–919)	2.2 ± 0.1	220
PDE3A (679–1087)	>10	>1000
PDE4D2 (86–413)	7.1 ± 0.3	710
PDE5A1 (535–860)	>10	>1000
PDE7A1 (130–482)	>10	>1000
PDE9A2 (181–506)	>10	>1000
PDE10A (449–770)	4.4 ± 0.2	440
PDE11A4 (588–911)	>10	>1000

Table 3. Pharmacokinetic Profile of 3a in SD Rats

	$t_{1/2}$ (h)	T_{max} (h)	C_{max} (ng/mL)	$AUC_{(0-t)}$ (h·ng/mL)	$AUC_{(0-\infty)}$ (h·ng/mL)	$MRT_{(0-t)}$ (h)	F (%)
i.v.	2.36 ± 0.39	0.14 ± 0.10	2192 ± 136	9410 ± 1157	9418 ± 1160	4.48 ± 0.25	
p.o.	2.82 ± 0.45	4.00 ± 0.00	1938 ± 317	17,459 ± 2691	17,592 ± 2792	7.20 ± 0.25	47 ± 7

PDE8A inhibitor **3a** possesses higher selectivity properties than other PDE isoforms.

Reasonable Druglike Profile. In view of its nanomolar inhibition against PDE8A and high selectivity across PDE isoforms, **3a** was further subjected to analysis of the water solubility, pharmacokinetic properties, human plasma binding rate, cytochrome P450 inhibition, human ether-a-go-go-related gene (hERG) inhibition, pK_a , $\log P$, and blood–brain barrier (BBB) permeability to characterize its physicochemical properties.

Oral administration (p.o.) of 10 mg/kg **3a** to SD rats resulted in a C_{max} of 1938 ng/mL, a $t_{1/2}$ of 2.82 h, a t_{max} of 4.00 h, an $AUC_{(0-\infty)}$ of 17,592 h·ng/mL, and an oral bioavailability of 47% (Table 3). Even after 24 h, its concentration in blood was over 30 ng/mL. The remarkable oral bioavailability and pharmacokinetic stability suggest that **3a** has the potential to be used as a lead compound for subsequent in vivo studies.

Other druglike profile evaluations of **3a** are shown in Table 4, such as water solubility [0.108 mg/mL using the high-

performance liquid chromatography (HPLC) method, pH 7.3], cytochrome P450 inhibition (IC_{50} values >25 μM against CYP1A2, 2C9, 2C19, 2D6, and 3A4-M), hERG inhibition (IC_{50} = 18 μM), and human plasma protein binding (PPB = 78%). Additionally, the values of pK_a and $\log P$ of **3a** are 3.69 and 3.84 (Figure S3), respectively, which are in the proper range of druggability. Calculated by the standard curve in the parallel artificial membrane permeation assay (PAMPA),³⁷ its BBB permeability (P_e = 6.0×10^{-6} cm/s) is greater than 3.6×10^{-6} cm/s and classified into the CNS+ range (Table S2), which suggests that **3a** is suitable for the in vivo VaD studies.

compound **3a** (3 mg/kg, p.o.) or donepezil (positive control, 1 mg/kg, p.o.), behavioral performance was evaluated. In the MWM test, the escape latency time (ELT) of each mouse to find the platform, the frequency of the platform site crossings, and the residence time in the platform were recorded on the spatial probe trial day to evaluate whether **3a** could improve the cognitive ability of each group.

The pharmacodynamics results in Figure 4 indicate that the UCCAO mouse model was successfully established relative to the control group, which resulted in cognitive impairment in UCCAO-treated mice. Remarkably, daily administration of compound **3a** and donepezil to mice significantly decreased the ELT and increased the residence time in the platform area and the frequency of platform site crossings. Meanwhile, the therapeutic effects of compound **3a** and donepezil was nearly. These phenomena strongly suggested that **3a** could improve vascular cognitive impairment and enhance the spatial learning and memory capability of the UCCAO-treated mice.

Moreover, the UCCAO-treated mice showed shortened avoidance latency and more error times in the passive avoidance test, while the trend improved in the **3a**- and donepezil-treated groups. Daily p.o. of **3a** and donepezil notably increased the avoidance latency and decreased the error times in the UCCAO-treated mice (Figure 5). The results of behavioral performance demonstrated that this compound could efficiently improve cognitive impairment in the UCCAO-treated mice and enhance learning and memory, which identified a PDE8A inhibitor as a novel agent for the effective treatment of VaD.

Table 4. Druglike Profile of Compound 3a

content	value
water solubility (pH 7.3, HPLC method)	0.108 mg/mL
Pharmacokinetic Properties (p.o.)	
$t_{1/2}$	2.82 h
F	47%
human plasma binding rate	78%
Cytochrome P450 Inhibition (IC_{50})	
CYP1A2, 2C9, 2C19, 2D6, and 3A4-M	>25 μM
hERG inhibition (IC_{50})	18 μM
pK_a	3.69
$\log P$	3.84
BBB permeability	$6.0 \pm 0.5 (\times 10^{-6})$ cm/s

performance liquid chromatography (HPLC) method, pH 7.3], cytochrome P450 inhibition (IC_{50} values >25 μM against CYP1A2, 2C9, 2C19, 2D6, and 3A4-M), hERG inhibition (IC_{50} = 18 μM), and human plasma protein binding (PPB = 78%). Additionally, the values of pK_a and $\log P$ of **3a** are 3.69 and 3.84 (Figure S3), respectively, which are in the proper range of druggability. Calculated by the standard curve in the parallel artificial membrane permeation assay (PAMPA),³⁷ its BBB permeability (P_e = 6.0×10^{-6} cm/s) is greater than 3.6×10^{-6} cm/s and classified into the CNS+ range (Table S2), which suggests that **3a** is suitable for the in vivo VaD studies.

Significant Pharmacodynamic Effects in the VaD Mice Model. To investigate whether compound **3a** could cause memory improvement in the VaD mice model, we used the Morris water maze (MWM) test and passive avoidance task. Mice by unilateral common carotid artery occlusion (UCCAO) were randomly assigned to three groups. Many studies suggest that donepezil was beneficial to treat cognitive impairment and memory deficits of VaD.^{38–41} Thus, donepezil was adopted as the positive control and to provide reference for the efficacy of compound **3a**. After 3 weeks of treatment with the vehicle (0.5% CMC–Na solution, p.o.) plus

CONCLUSIONS

In summary, medicinal chemistry optimizations targeting Tyr748 in PDE8A identified the most potent inhibitor **3a** (IC_{50} = 0.010 μM) with high selectivity across PDE isoforms and a reasonable druglike profile. The X-ray crystal structure of PDE8A–**3a** revealed the first binding pattern of a selective inhibitor with PDE8A after the report of PDE8A–IBMX (pan-PDE inhibitor) more than a decade ago, which may explain the improvement of the selectivity index of 220-fold against PDE2A compared to that of clofarabine (26-fold). Our work thus validated that Tyr748 is a crucial residue for the discovery of highly effective PDE8A inhibitors.

Furthermore, p.o. of **3a** caused comparable therapeutic effects to donepezil against VaD. These results suggest that selective PDE8A inhibitors could provide remarkable alternative compounds for the effective treatment of VaD.

EXPERIMENTAL SECTION

General Methods. All the materials and reagents were bought from commercial agents (Bide, Energy and Meryer) without further purification. Chemical HG/T2354-92 silica gel (200–300 mesh, Haiyang) was used for chromatography, and silica gel plates with fluorescence F254 (0.25 mm, Huanghai) were used for thin-layer chromatography analysis. Reactions under anoxic stress were performed under argon. NMR spectra were recorded at room temperature on a Bruker Ascend 500, operating at 500 MHz for ¹H NMR and 126 MHz for ¹³C NMR, or a Bruker Avance III, operating at 400 MHz for ¹H NMR and 101 MHz for ¹³C NMR. The following

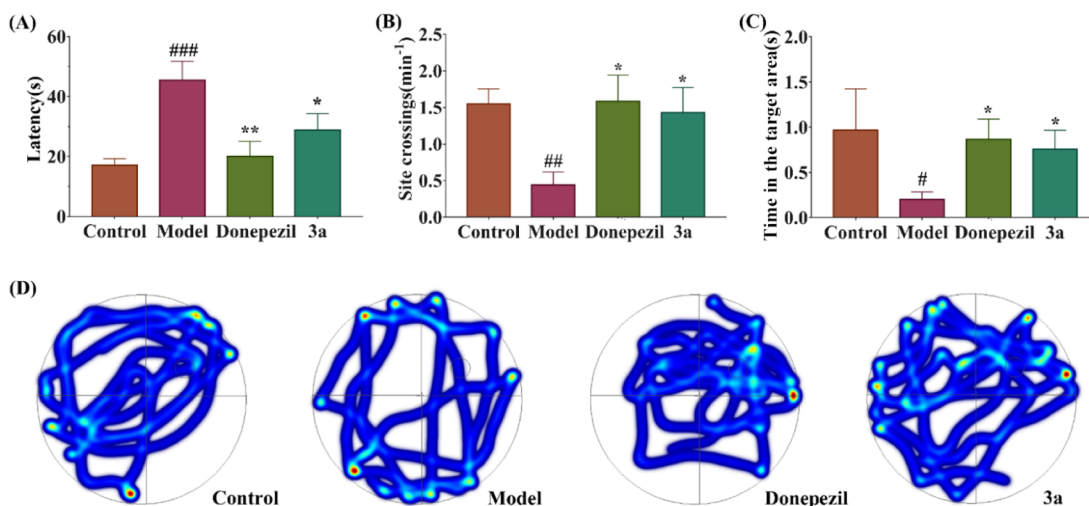


Figure 4. Spatial learning and memory improvement of compound 3a to UCCAO-treated mice after 3 weeks at the oral dose of 3 mg/kg. (A) ELT of UCCAO-treated mice in the spatial probe trial (s). (B) Frequency of the platform site crossings in the spatial probe trial (min^{-1}). (C) Swimming time in the target area in the spatial probe trial (s). (D) Representative swimming trajectories of each group in the spatial probe trial. Donepezil (1 mg/kg, p.o.) was used as the positive control. Data are presented as the mean \pm SEM. UCCAO-treated mice in each group, $n = 9-12$. #, $p < 0.05$ vs control; ##, $p < 0.01$ vs control; ###, $p < 0.001$ vs control; *, $p < 0.05$ vs model; **, $p < 0.01$ vs model.

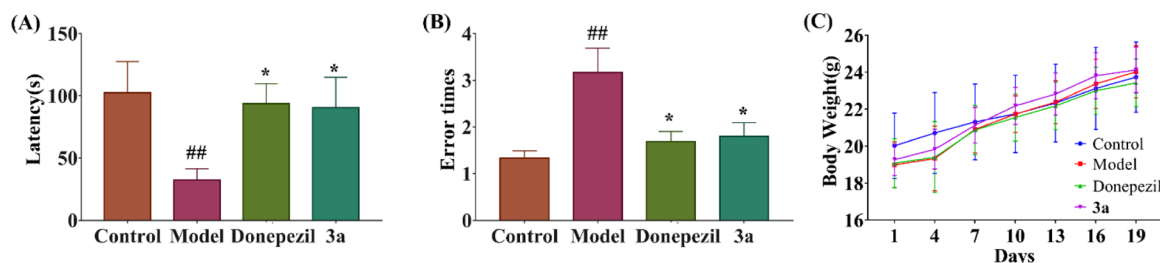


Figure 5. Therapeutic effects of compound 3a on escaping reaction acquisition in the passive avoidance task in UCCAO mice. (A) Avoidance latency time of the passive avoidance task (s). (B) Error times of the passive avoidance task. Data are presented as the mean \pm SEM. UCCAO-treated mice in each group, $n = 9-12$. #, $p < 0.05$ vs control; ##, $p < 0.01$ vs control; *, $p < 0.05$ vs model. (C) Body weight of different groups.

abbreviations are used: s (singlet), br (broad signal), d (doublet), dd (doublet of doublets), t (triplet), q (quartet), and m (multiplet). Coupling constants are reported in hertz (Hz). High-resolution mass spectra were recorded on a MAT-95 spectrometer. The purity of targeted compounds was more than 95%, which was determined by reverse-phase HPLC analysis. HPLC instrument: SHIMADZU LC-20AT [column: Hypersil BDS C18, 5.0 μm , 4.6 \times 150 mm (Elite)]; detector: SPD-20A UV/vis detector, UV detection at 254 nm; elution, CH_3CN in water (60–70%, v/v); $T = 25^\circ\text{C}$; and flow rate = 1.0 mL/min.

General Procedure for Synthesis of Intermediates M3a–d.

To the solution of M1 (2.4 mmol) and M2 (2 mmol) in 1,4-dioxane/ H_2O (4:1, 5 mL), K_2CO_3 (4 mmol) and $\text{Pd}(\text{dppf})\text{Cl}_2 \cdot \text{CH}_2\text{Cl}_2$ (0.4 mmol) were added. The mixture was stirred at 100°C overnight under an atmosphere of Ar. After the mixture was cooled to room temperature (r.t.), it was diluted with water and extracted with ethyl acetate (EA) three times. The combined organic extracts were dried over anhydrous Na_2SO_4 and concentrated to give a crude product, which was purified by silica gel column chromatography [petroleum ether (PE)/EA, 3:1] to get M3a–d.

(6-(Furan-2-yl)pyridin-2-yl)methanol (M3a). Yield: 83%. ^1H NMR (400 MHz, CDCl_3): δ 7.71 (t, $J = 7.8$ Hz, 1H), 7.60 (d, $J = 7.8$ Hz, 1H), 7.55–7.50 (m, 1H), 7.09 (dd, $J = 4.0, 3.4$ Hz, 2H), 6.54 (dd, $J = 3.4, 1.8$ Hz, 1H), 4.77 (d, $J = 4.5$ Hz, 2H), 3.88 (t, $J = 4.9$ Hz, 1H).

(6-(2-Fluorophenyl)pyridin-2-yl)methanol (M3b). Yield: 57%. ^1H NMR (400 MHz, CDCl_3): δ 8.01 (t, $J = 7.9$ Hz, 1H), 7.80–7.70 (m, 2H), 7.40 (dd, $J = 13.2, 5.8$ Hz, 1H), 7.29 (d, $J = 7.5$ Hz, 1H), 7.23–7.14 (m, 2H), 4.83 (s, 2H), 3.96 (s, 1H).

(6-(Cyclopent-1-en-1-yl)pyridin-2-yl)methanol (M3c). Yield: 61%.

^1H NMR (400 MHz, CDCl_3): δ 7.61 (t, $J = 7.7$ Hz, 1H), 7.26 (s, 1H), 7.01 (d, $J = 7.7$ Hz, 1H), 6.66 (dd, $J = 4.4, 2.3$ Hz, 1H), 4.73 (s, 2H), 4.27 (s, 1H), 2.80 (ddd, $J = 10.0, 4.6, 2.2$ Hz, 2H), 2.59 (dtd, $J = 10.1, 4.9, 2.4$ Hz, 2H), 2.10–2.03 (m, 2H).

(6-(3,6-Dihydro-2H-pyran-4-yl)pyridin-2-yl)methanol (M3d).

Yield: 80%. ^1H NMR (400 MHz, CDCl_3): δ 7.66 (t, $J = 7.7$ Hz, 1H), 7.29 (d, $J = 7.9$ Hz, 1H), 7.08 (d, $J = 7.6$ Hz, 1H), 6.75 (ddd, $J = 4.4, 3.0, 1.4$ Hz, 1H), 4.75 (d, $J = 4.3$ Hz, 2H), 4.39 (dd, $J = 5.3, 2.6$ Hz, 2H), 4.08 (t, $J = 4.5$ Hz, 1H), 3.96 (t, $J = 5.4$ Hz, 2H), 2.66 (qd, $J = 5.3, 2.4$ Hz, 2H).

Procedures for the Synthesis of Intermediate M3e. Sodium 2,2-difluoroethanolate (6 mmol) was added to the solution of M2 (3 mmol) in 2,2-difluoroethanol (3 mL). The mixture was stirred at 90°C for 40 h. The mixture was diluted with water and extracted with dichloromethane (DCM) three times. The combined organic layers were dried over anhydrous Na_2SO_4 , concentrated in vacuo, and purified by silica gel column chromatography (PE/EA, 5:1) to give M3e.

(6-(2,2-Difluoroethoxy)pyridin-2-yl)methanol (M3e). Yield: 19%. ^1H NMR (400 MHz, CDCl_3): δ 7.62 (dd, $J = 8.1, 7.5$ Hz, 1H), 6.92 (dd, $J = 7.3, 0.6$ Hz, 1H), 6.73 (dd, $J = 8.2, 0.5$ Hz, 1H), 6.12 (tt, $J = 55.4, 4.2$ Hz, 1H), 4.68 (d, $J = 5.2$ Hz, 2H), 4.56 (td, $J = 13.6, 4.2$ Hz, 2H), 2.97 (t, $J = 5.4$ Hz, 1H).

General Procedures for the Synthesis of Intermediates M4c–g. PBr_3 (150 μL) was added dropwise to a stirred solution of M3a–e (2 mmol) in dry DCM (20 mL) at 0°C . The reaction mixture was stirred for 4 h at r.t. and quenched by addition of a saturated solution of NaHCO_3 and DCM. The organic layer was dried

over anhydrous Na₂SO₄ and evaporated in vacuo to afford the crude product.

2-(Bromomethyl)-6-(furan-2-yl)pyridine (M4c). Yield: 73%. ¹H NMR (400 MHz, CDCl₃): δ 7.71 (t, *J* = 7.8 Hz, 1H), 7.59 (d, *J* = 7.2 Hz, 1H), 7.54 (dd, *J* = 1.7, 0.7 Hz, 1H), 7.32 (dd, *J* = 7.7, 0.8 Hz, 1H), 7.09 (dd, *J* = 3.4, 0.7 Hz, 1H), 6.53 (dd, *J* = 3.4, 1.8 Hz, 1H), 4.57 (s, 2H).

2-(Bromomethyl)-6-(2-fluorophenyl)pyridine (M4d). Yield: 86%. ¹H NMR (400 MHz, CDCl₃): δ 8.03 (td, *J* = 7.9, 1.8 Hz, 1H), 7.75 (dt, *J* = 15.8, 8.0 Hz, 2H), 7.43 (d, *J* = 7.4 Hz, 1H), 7.41–7.35 (m, 1H), 7.28 (d, *J* = 8.5 Hz, 1H), 7.16 (dd, *J* = 11.4, 8.2 Hz, 1H), 4.63 (s, 2H).

2-(Bromomethyl)-6-(cyclopent-1-en-1-yl)pyridine (M4e). Yield: 84%. ¹H NMR (400 MHz, CDCl₃): δ 7.64 (t, *J* = 7.8 Hz, 1H), 7.30 (s, 1H), 7.25 (d, *J* = 7.8 Hz, 1H), 6.70–6.66 (m, 1H), 4.56 (s, 2H), 2.80 (ddd, *J* = 10.0, 4.6, 2.2 Hz, 2H), 2.59 (dtd, *J* = 10.1, 4.9, 2.4 Hz, 2H), 2.13–1.99 (m, 2H).

2-(Bromomethyl)-6-(3,6-dihydro-2H-pyran-4-yl)pyridine (M4f). Yield: 81%. ¹H NMR (400 MHz, CDCl₃): δ 7.67 (d, *J* = 7.8 Hz, 1H), 7.32 (d, *J* = 7.7 Hz, 1H), 7.28 (s, 1H), 6.75 (tt, *J* = 3.5, 1.8 Hz, 1H), 4.54 (s, 2H), 4.38 (dd, *J* = 5.6, 2.8 Hz, 2H), 3.94 (t, *J* = 5.5 Hz, 2H), 2.64 (td, *J* = 5.3, 2.6 Hz, 2H).

2-(Bromomethyl)-6-(2,2-difluoroethoxy)pyridine (M4g). Yield: 75%. ¹H NMR (500 MHz, CDCl₃): δ 7.60 (t, *J* = 7.7 Hz, 1H), 7.05 (d, *J* = 7.1 Hz, 1H), 6.74 (d, *J* = 8.2 Hz, 1H), 6.31–6.00 (m, 1H), 4.56 (td, *J* = 13.3, 3.7 Hz, 2H), 4.43 (s, 2H).

General Procedures for the Synthesis of Compounds 1a–f and 1i. M4a–g (1 mmol) and 2-chloro-9H-purin-6-amine (1 mmol) were dissolved in DMF. Cs₂CO₃ (2 mmol) was added to the mixture and then stirred at 70 °C overnight. The mixture was diluted with water, extracted with EA, and washed with brine. The combined organic layers were dried over anhydrous Na₂SO₄, concentrated under reduced pressure, and purified by silica gel column chromatography or recrystallization to give 1a–f and 1i as a white or yellow solid.

2-Chloro-9-(pyridin-2-ylmethyl)-9H-purin-6-amine (1a). Yield: 58%. Purity: 98%. ¹H NMR (400 MHz, DMSO-*d*₆): δ 8.55 (d, *J* = 4.7 Hz, 1H), 8.29 (s, 1H), 7.87 (d, *J* = 7.7 Hz, 1H), 7.81 (s, 2H), 7.38 (dd, *J* = 7.2, 5.1 Hz, 1H), 7.33 (d, *J* = 7.8 Hz, 1H), 5.52 (s, 2H). ¹³C NMR (101 MHz, DMSO-*d*₆): δ 157.2, 155.8, 153.5, 151.2, 149.8, 142.6, 137.7, 123.4, 122.0, 118.1, 48.1. HRMS (ESI-TOF) *m/z*: [M + H]⁺ calcd for C₁₁H₉ClN₆, 261.0650; found, 261.0646.

2-Chloro-9-((6-methylpyridin-2-yl)methyl)-9H-purin-6-amine (1b). Yield: 60%. Purity: 98%. ¹H NMR (400 MHz, CDCl₃): δ 8.02 (s, 1H), 7.70 (t, *J* = 7.9 Hz, 1H), 7.22 (d, *J* = 8.0 Hz, 2H), 5.39 (s, 2H), 2.56 (s, 3H). ¹³C NMR (126 MHz, DMSO-*d*₆): δ 161.7, 158.3, 155.1, 153.3, 153.2, 147.5, 138.9, 123.6, 120.3, 110.9, 51.4, 24.0. HRMS (ESI-TOF) *m/z*: [M + H]⁺ calcd for C₁₂H₁₁ClN₆, 275.0806; found, 275.0801.

2-Chloro-9-((6-(furan-2-yl)pyridin-2-yl)methyl)-9H-purin-6-amine (1c). Yield: 56%. Purity: 98%. ¹H NMR (400 MHz, CDCl₃): δ 8.08 (s, 1H), 7.71 (t, *J* = 7.8 Hz, 1H), 7.63 (d, *J* = 7.6 Hz, 1H), 7.55 (d, *J* = 1.0 Hz, 1H), 7.13 (d, *J* = 7.5 Hz, 1H), 7.03 (d, *J* = 3.1 Hz, 1H), 6.54 (dd, *J* = 3.4, 1.8 Hz, 1H), 6.04 (s, 2H), 5.48 (s, 2H). ¹³C NMR (101 MHz, CDCl₃): δ 156.2, 154.3, 154.3, 153.2, 151.3, 149.4, 143.6, 141.6, 137.9, 120.2, 118.1, 117.9, 112.1, 109.4, 48.6. HRMS (ESI-TOF) *m/z*: [M + H]⁺ calcd for C₁₅H₁₁ClN₆O, 327.0756; found, 327.0751.

2-Chloro-9-((6-(2-fluorophenyl)pyridin-2-yl)methyl)-9H-purin-6-amine (1d). Yield: 61%. Purity: 99%. ¹H NMR (400 MHz, CDCl₃): δ 8.09 (s, 1H), 7.91 (td, *J* = 7.9, 1.8 Hz, 1H), 7.78–7.73 (m, 2H), 7.37–7.43 (m, 1H), 7.23–7.29 (m, 2H), 7.16 (ddd, *J* = 11.4, 8.2, 1.0 Hz, 1H), 6.09 (s, 2H), 5.52 (s, 2H). ¹³C NMR (101 MHz, CDCl₃): δ 160.6 (d, *J* = 250.4 Hz), 156.3, 154.3, 153.5, 151.3, 141.6, 137.7, 130.90 (d, *J*_{C–F} = 2.4 Hz), 130.8 (d, *J*_{C–F} = 8.7 Hz), 126.8, 124.6 (d, *J*_{C–F} = 3.2 Hz), 124.0 (d, *J*_{C–F} = 9.6 Hz), 120.9, 118.1, 116.4, 116.2, 48.7. HRMS (ESI-TOF) *m/z*: [M + H]⁺ calcd for C₁₇H₁₂ClFN₆O, 355.0869; found, 355.0858.

2-Chloro-9-((6-(cyclopent-1-en-1-yl)pyridin-2-yl)methyl)-9H-purin-6-amine (1e). Yield: 61%. Purity: 99%. ¹H NMR (400 MHz, MeOD): δ 8.20 (s, 1H), 7.68 (t, *J* = 7.8 Hz, 1H), 7.38 (d, *J* = 7.9 Hz,

1H), 7.12 (d, *J* = 7.7 Hz, 1H), 6.52–6.46 (m, 1H), 5.46 (s, 2H), 2.66 (ddt, *J* = 10.0, 7.6, 2.3 Hz, 2H), 2.52 (dtd, *J* = 10.2, 5.1, 2.5 Hz, 2H), 2.04–1.90 (m, 3H). ¹³C NMR (101 MHz, CDCl₃): δ 156.0, 155.3, 154.1, 153.6, 151.4, 143.1, 141.9, 137.2, 132.1, 119.7, 119.6, 118.1, 48.6, 33.5, 32.5, 23.3. HRMS (ESI-TOF) *m/z*: [M + H]⁺ calcd for C₁₆H₁₅ClN₆, 327.1119; found, 327.1117.

2-Chloro-9-((6-(3,6-dihydro-2H-pyran-4-yl)pyridin-2-yl)methyl)-9H-purin-6-amine (1f). Yield: 55%. Purity: 99%. ¹H NMR (400 MHz, MeOD): δ 8.20 (s, 1H), 7.73 (t, *J* = 7.8 Hz, 1H), 7.43 (d, *J* = 8.0 Hz, 1H), 7.20 (d, *J* = 7.7 Hz, 1H), 6.61 (ddd, *J* = 4.3, 2.7, 1.5 Hz, 1H), 5.48 (s, 2H), 4.28 (dd, *J* = 5.5, 2.8 Hz, 2H), 3.85 (t, *J* = 5.5 Hz, 2H), 2.46 (ddt, *J* = 7.4, 4.7, 2.4 Hz, 2H). ¹³C NMR (126 MHz, CDCl₃): δ 156.8, 156.1, 154.2, 153.4, 151.3, 141.7, 137.6, 133.8, 126.8, 120.3, 118.2, 118.1, 65.8, 64.4, 48.5, 25.7. HRMS (ESI-TOF) *m/z*: [M + H]⁺ calcd for C₁₆H₁₅ClN₆O, 343.1069; found, 343.1068.

2-Chloro-9-((6-(2,2-difluoroethoxy)pyridin-2-yl)methyl)-9H-purin-6-amine (1i). Yield: 54%. Purity: 98%. ¹H NMR (400 MHz, MeOD): δ 8.20 (s, 1H), 7.70 (dd, *J* = 8.2, 7.4 Hz, 1H), 6.99 (d, *J* = 7.3 Hz, 1H), 6.76 (d, *J* = 8.3 Hz, 1H), 5.99 (tt, *J* = 55.6, 4.1 Hz, 1H), 5.42 (s, 2H), 4.31 (td, *J* = 13.9, 4.1 Hz, 2H). ¹³C NMR (126 MHz, CDCl₃): δ 166.8, 162.0, 158.3, 158.3, 156.0, 147.3, 146.1, 122.8, 120.4, 119.0 (t, *J*_{C–F} = 239.1 Hz), 114.9, 68.6 (t, *J*_{C–F} = 27.7 Hz), 52.3. HRMS (ESI-TOF) *m/z*: [M + H]⁺ calcd for C₁₃H₁₁ClF₂N₆O, 341.0724; found, 341.0721.

General Procedures for the Synthesis of Compounds 1g–h.

10% Pd/C (10%, w/w) was added to the solution of 1e–f (0.5 mmol) in MeOH/tetrahydrofuran (THF) (20 mL, 1:1, v/v). The reaction mixture was stirred at r.t. overnight under an atmosphere of H₂. The mixture was then filtered through Celite, and the solvent was removed in vacuo to afford the crude product, which was purified by silica gel column chromatography to give 1g–h as a white solid.

2-Chloro-9-((6-cyclopentylpyridin-2-yl)methyl)-9H-purin-6-amine (1g). Yield: 83%. Purity: 96%. ¹H NMR (400 MHz, CDCl₃): δ 8.05 (s, 1H), 7.55 (t, *J* = 7.7 Hz, 1H), 7.10 (d, *J* = 7.7 Hz, 1H), 7.05 (d, *J* = 7.6 Hz, 1H), 5.96 (s, 2H), 5.40 (s, 2H), 3.20–3.09 (m, 1H), 2.07–1.99 (m, 2H), 1.79 (d, *J* = 2.6 Hz, 1H), 1.74–1.61 (m, 5H). ¹³C NMR (101 MHz, CDCl₃): δ 166.3, 156.2, 154.1, 153.4, 151.3, 141.7, 137.2, 121.2, 119.3, 118.0, 48.6, 47.6, 33.5, 25.8. HRMS (ESI-TOF) *m/z*: [M + H]⁺ calcd for C₁₆H₁₇ClN₆, 329.1276; found, 329.1279.

2-Chloro-9-((6-(tetrahydro-2H-pyran-4-yl)pyridin-2-yl)methyl)-9H-purin-6-amine (1h). Yield: 88%. Purity: 99%. ¹H NMR (400 MHz, CDCl₃): δ 8.04 (s, 1H), 7.61 (t, *J* = 7.7 Hz, 1H), 7.11 (d, *J* = 7.7 Hz, 2H), 5.93 (s, 2H), 5.41 (s, 2H), 4.08 (ddd, *J* = 11.7, 4.0, 2.0 Hz, 2H), 3.54 (td, *J* = 11.5, 2.9 Hz, 2H), 2.91 (ddd, *J* = 15.6, 11.0, 4.6 Hz, 1H), 1.92–1.79 (m, 4H). ¹³C NMR (101 MHz, CDCl₃): δ 164.7, 156.3, 154.2, 153.8, 151.2, 141.6, 137.7, 120.5, 119.8, 118.1, 68.0, 48.6, 43.1, 32.2. HRMS (ESI-TOF) *m/z*: [M + H]⁺ calcd for C₁₆H₁₇ClN₆O, 345.1225; found, 345.1226.

General Procedures for the Synthesis of Intermediates M6a–b.

M6a–b were synthesized by the general procedure for the synthesis of M3e.

(4-Methoxypyridin-2-yl)methanol (M6a). Yield: 96%. ¹H NMR (400 MHz, CDCl₃): δ 8.37 (t, *J* = 4.9 Hz, 1H), 6.78 (d, *J* = 2.0 Hz, 1H), 6.74 (dd, *J* = 5.7, 2.4 Hz, 1H), 4.71 (s, 2H), 3.86 (s, 3H).

(4-(2,2-Difluoroethoxy)pyridin-2-yl)methanol (M6b). Yield: 36%. ¹H NMR (400 MHz, CDCl₃): δ 8.42 (d, *J* = 5.7 Hz, 1H), 6.85 (d, *J* = 2.3 Hz, 1H), 6.78 (dd, *J* = 5.7, 2.5 Hz, 1H), 6.12 (tt, *J* = 54.8, 4.0 Hz, 1H), 4.74 (s, 2H), 4.26 (td, *J* = 12.9, 4.0 Hz, 2H).

General Procedures for the Synthesis of Intermediates M7a–c.

M7a–c were synthesized by the general procedure for the synthesis of M4c–g.

2-(Bromomethyl)-4-chloropyridine (M7a). Yield: 83%. ¹H NMR (400 MHz, CDCl₃): δ 8.48 (d, *J* = 5.3 Hz, 1H), 7.47 (d, *J* = 1.7 Hz, 1H), 7.24 (dd, *J* = 5.3, 1.8 Hz, 1H), 4.51 (s, 2H).

2-(Bromomethyl)-4-methoxypyridine (M7b). Yield: 88%. ¹H NMR (400 MHz, CDCl₃): δ 8.41 (d, *J* = 5.8 Hz, 1H), 6.98 (d, *J* = 2.4 Hz, 1H), 6.76 (dd, *J* = 5.8, 2.4 Hz, 1H), 4.52 (s, 2H), 3.89 (s, 3H).

2-(Bromomethyl)-4-(2,2-difluoroethoxy)pyridine (M7c). Yield: 81%. ¹H NMR (400 MHz, CDCl₃): δ 8.46 (d, *J* = 5.7 Hz, 1H),

7.02 (d, $J = 2.3$ Hz, 1H), 6.78 (dd, $J = 5.7, 2.4$ Hz, 1H), 6.13 (tt, $J = 54.8, 4.0$ Hz, 1H), 4.52 (s, 2H), 4.27 (td, $J = 12.8, 4.0$ Hz, 2H).

General Procedures for the Synthesis of Compounds 2a–c. 2a–c were synthesized by the general procedure for the synthesis of 1a–f and 1i.

2-Chloro-9-((4-chloropyridin-2-yl)methyl)-9H-purin-6-amine (2a). Yield: 52%. Purity: 98%. ^1H NMR (400 MHz, CDCl_3): δ 8.46 (d, $J = 5.3$ Hz, 1H), 7.98 (s, 1H), 7.28 (m, 2H), 6.02 (s, 2H), 5.43 (s, 2H). ^{13}C NMR (126 MHz, $\text{DMSO}-d_6$): δ 157.9, 157.2, 153.5, 151.3, 151.2, 144.1, 142.6, 123.6, 122.3, 118.1, 47.6. HRMS (ESI-TOF) m/z : $[\text{M} + \text{H}]^+$ calcd for $\text{C}_{11}\text{H}_8\text{Cl}_2\text{N}_6$, 295.0260; found, 295.0259.

2-Chloro-9-((4-methoxy-pyridin-2-yl)methyl)-9H-purin-6-amine (2b). Yield: 55%. Purity: 98%. ^1H NMR (400 MHz, CDCl_3): δ 8.38 (d, $J = 5.7$ Hz, 1H), 7.98 (s, 1H), 6.85 (d, $J = 2.3$ Hz, 1H), 6.75 (dd, $J = 5.8, 2.4$ Hz, 1H), 5.80 (s, 2H), 5.38 (s, 2H), 3.83 (s, 3H). ^{13}C NMR (126 MHz, MeOD): δ 167.3, 156.7, 156.4, 154.0, 150.8, 150.4, 141.9, 117.4, 109.1, 108.7, 54.7, 47.7. HRMS (ESI-TOF) m/z : $[\text{M} + \text{H}]^+$ calcd for $\text{C}_{12}\text{H}_{11}\text{ClN}_6\text{O}$, 291.0756; found, 291.0756.

2-Chloro-9-((4-(2,2-difluoroethoxy)pyridin-2-yl)methyl)-9H-purin-6-amine (2c). Yield: 58%. Purity: 99%. ^1H NMR (400 MHz, CDCl_3): δ 8.43 (d, $J = 5.7$ Hz, 1H), 7.98 (s, 1H), 6.89 (d, $J = 2.3$ Hz, 1H), 6.78 (dd, $J = 5.7, 2.4$ Hz, 1H), 5.85–6.23 (m, 3H), 5.40 (s, 2H), 4.22 (td, $J = 12.8, 4.0$ Hz, 2H). ^{13}C NMR (126 MHz, MeOD): δ 165.4, 156.7, 156.7, 154.0, 150.8, 150.7, 142.0, 117.4, 113.5 (t, $J_{\text{C-F}} = 239.7$ Hz), 109.4, 109.0, 66.6 (t, $J_{\text{C-F}} = 28.7$ Hz), 47.7. HRMS (ESI-TOF) m/z : $[\text{M} + \text{H}]^+$ calcd for $\text{C}_{13}\text{H}_{11}\text{ClF}_2\text{N}_6\text{O}$, 341.0724; found, 341.0721.

Procedures for the Synthesis of Intermediate M9. M9 was synthesized by the general procedure for the synthesis of M3e.

2-Chloro-4-(2,2-difluoroethoxy)pyridine (M9). Yield: 52%. ^1H NMR (400 MHz, CDCl_3): δ 8.25 (d, $J = 5.8$ Hz, 1H), 6.88 (d, $J = 2.2$ Hz, 1H), 6.80 (dd, $J = 5.8, 2.0$ Hz, 1H), 6.10 (tt, $J = 54.8, 4.1$ Hz, 1H), 4.24 (td, $J = 12.8, 4.0$ Hz, 2H).

Procedures for the Synthesis of Intermediate M10. M10 was synthesized by the general procedure for the synthesis of M3a–e.

4-(2,2-Difluoroethoxy)-2-vinylpyridine (M10). Yield: 95%. ^1H NMR (400 MHz, CDCl_3): δ 8.44 (d, $J = 5.7$ Hz, 1H), 6.87 (d, $J = 2.5$ Hz, 1H), 5.96–6.26 (m, 2H), 6.26–5.95 (m, 2H), 5.50 (dd, $J = 10.8, 1.1$ Hz, 1H), 4.25 (td, $J = 12.9, 4.1$ Hz, 2H).

Procedures for the Synthesis of Intermediate M11. M11 was synthesized by the general procedure for the synthesis of 1g–h.

4-(2,2-Difluoroethoxy)-2-ethylpyridine (M11). Yield: 100%. ^1H NMR (400 MHz, CDCl_3): δ 8.41 (d, $J = 5.7$ Hz, 1H), 6.73 (d, $J = 2.4$ Hz, 1H), 6.68 (dd, $J = 5.7, 2.5$ Hz, 1H), 6.12 (tt, $J = 54.9, 4.1$ Hz, 1H), 4.24 (td, $J = 12.9, 4.1$ Hz, 2H), 2.82 (q, $J = 7.6$ Hz, 2H), 1.32 (t, $J = 7.6$ Hz, 3H).

Procedures for the Synthesis of Intermediate M12. NBS (10 mmol) and 2,2'-azo-bis-isobutyronitrile (AIBN) (0.5 mmol) were added to the solution of M11 (10 mmol) in CCl_4 (100 mL). The reaction mixture was stirred for 4 h at reflux under an atmosphere of Ar. The mixture was then filtered, concentrated, and purified by silica gel column chromatography (PE/EA, 5:1) to get M12.

2-(1-Bromoethyl)-4-(2,2-difluoroethoxy)pyridine (M12). Yield: 81%. ^1H NMR (500 MHz, CDCl_3): δ 8.44 (d, $J = 5.7$ Hz, 1H), 7.01 (d, $J = 2.4$ Hz, 1H), 6.75 (dd, $J = 5.7, 2.5$ Hz, 1H), 6.11 (tt, $J = 54.8, 4.0$ Hz, 1H), 5.18 (q, $J = 6.9$ Hz, 1H), 4.26 (td, $J = 12.8, 4.0$ Hz, 2H), 2.06 (d, $J = 6.9$ Hz, 3H).

Procedures for the Synthesis of Compound 3. 3 was synthesized by the general procedure for the synthesis of 1a–f and 1i.

2-Chloro-9-(1-(4-(2,2-difluoroethoxy)pyridin-2-yl)ethyl)-9H-purin-6-amine (3). Yield: 56%. Purity: 98%. ^1H NMR (400 MHz, CDCl_3): δ 8.45 (d, $J = 5.7$ Hz, 1H), 8.19 (s, 1H), 6.94 (d, $J = 2.4$ Hz, 1H), 6.77 (dd, $J = 5.7, 2.5$ Hz, 1H), 6.25–5.83 (m, 4H), 4.23 (td, $J = 12.8, 4.0$ Hz, 2H), 1.95 (d, $J = 7.2$ Hz, 3H). ^{13}C NMR (126 MHz, CDCl_3): δ 164.5, 160.2, 156.0, 153.9, 151.4, 150.9, 140.0, 118.1, 112.9 (t, $J_{\text{C-F}} = 241.8$ Hz), 109.4, 108.8, 84.5, 66.7 (t, $J_{\text{C-F}} = 29.9$ Hz), 54.7, 20.8. HRMS (ESI-TOF) m/z : $[\text{M} + \text{H}]^+$ calcd for $\text{C}_{14}\text{H}_{13}\text{ClF}_2\text{N}_6\text{O}$, 355.0880; found, 355.0877. Daicel CHIRALPAK AD-3 (0.46 cm \times 25 cm); hexane/isopropanol = 55/45; flow rate = 1 mL/min; detection wavelength = 254 nm; $t_1 = 9.30$ min, (S)-3/3a; t_2

= 10.10 min, (R)-3/3b; (S)-3, $[\alpha]_D^{20} -74.0$ (c 0.1, CHCl_3), ee > 99%; (R)-3, $[\alpha]_D^{20} 74.0$ (c 0.1, CHCl_3), ee > 99%.

Molecular Docking. The Surflex-Dock suite⁴² of Tripos Sybyl-X.2.0 was used to predict the binding modes between designed compounds and PDE8A. The active site was represented by the ProtoMol, which was based on the bound ligand IBMX within PDE8A (PDB ID: 3ECN). The parameters of proto_bloat and proto_thresh were set to 0 and 0.5, respectively. In addition, other parameters were assigned default values. A total of 20 poses of each compound were generated for analysis.

Protein Expression and Purification. The recombinant pET15b-PDE8A1 plasmid (catalytic domain, 480–820) was subcloned and purified by protocols reported previously.^{36,43} The recombinant plasmid was transferred into the *Escherichia coli* strain BL21 (CodonPlus, DE3). Then, the *E. coli* cells carrying the plasmid grew in the 2 \times YT medium (containing 100 mg/mL ampicillin, 50 mg/mL chloramphenicol, and 0.4% glucose) at 37 $^\circ\text{C}$ until $\text{OD}_{600} = 0.6$ –0.8, and then, 0.1 mM isopropyl- β -D-thiogalactopyranoside was added to induce the PDE8A1 protein overexpression. The induced cells were collected after growing at 25 $^\circ\text{C}$ for another 20–24 h. The pellet from the frozen cells was denatured in the buffer of 7.8 M guanidine and 0.1 M Tris-HCl pH 8.0 overnight. A nickel nitriloacetic acid column (Qiagen) was used to purify the dissolved supernatant. The elution protein at a 30 $\mu\text{g}/\text{mL}$ concentration was added dropwise into the refolding buffer under mild stir. The refolding was carried out at the 30 $\mu\text{g}/\text{mL}$ protein concentration without shaking at 4 $^\circ\text{C}$ for 3 days. The recombinant PDE8A1 protein was purified using hydroxyapatite HTP GEL (Bio-Rad), a Q Sepharose column (GE Healthcare), and a gel filtration column Sephacryl S₁₀₀ (GE Healthcare). A typical batch of purification yielded 4–10 mg of the PDE8A1 protein from a 6 L cell culture medium. The PDE8A1 proteins had a purity greater than 95%, as shown by the sodium dodecyl sulfate gel. The proteins were used for the enzymatic activity assay of compounds, crystallization, and structure determination of PDE8A–clofarabine/2a/3c (Table S3).

The fragments of PDE1B (146–506, delete 449–471), PDE2A (580–919), PDE3A (679–1087), PDE4D (86–413), PDE5A (535–860), PDE7A (130–482), PDE9A (181–506), and PDE10A (449–770) were purified by using similar protocols but without the denaturing and refolding processes as previously reported.^{15,30,44–51}

The same procedures (Supporting Information) for the enzymology and crystallization trials were performed as previous studies.^{15,30,44–51}

Druglike Profile Determinations. The same procedures for the druglike profile determinations such as pharmacokinetic properties, plasma protein binding rate, cytochrome P450 inhibition, hERG inhibition, pK_a , log P , and PAMPA–BBB (Supporting Information) were performed as our previous studies.^{15,45,48–52}

UCCAO Mouse Model of VaD and the MWM Test. The same protocols as reported in our previous work have been performed^{15,51} (Supporting Information) for the UCCAO mouse model of VaD and the MWM test. All animal care and experimental protocols were in accordance with the “Guide for the Care and Use of Laboratory Animals” (National Institutes of Health Publication, revised 1996, no. 86-23, Bethesda, MD) and approved by the Institutional Ethical Committee for Animal Research of Sun Yat-Sen University (IACUC number: SYSU-IACUC-2020-000292).

■ ASSOCIATED CONTENT

Supporting Information

The Supporting Information is available free of charge at <https://pubs.acs.org/doi/10.1021/acs.jmedchem.0c01573>.

Molecular formula strings and some data (CSV)

In vivo pharmacokinetics analysis; druglike profile of compound 3a; PAMPA–BBB procedures; general procedures for crystallization trials; ^1H NMR, ^{13}C NMR, and high-resolution mass spectra data for targeted compounds; and purity of the tested compounds (PDF)

Accession Codes

The atomic coordinates and structure factors have been deposited into the RCSB Protein Data Bank with accession numbers 7CWA, 7CWF, and 7CWG. Authors will release the atomic coordinates and experimental data upon article publication.

AUTHOR INFORMATION

Corresponding Author

Hai-Bin Luo – School of Pharmaceutical Sciences, Sun Yat-Sen University, Guangzhou 510006, P. R. China; Key Laboratory of Tropical Biological Resources of Ministry of Education, School of Life and Pharmaceutical Sciences, Hainan University, Haikou 570228, Hainan, China; orcid.org/0000-0002-2163-0509; Email: luohb77@mail.sysu.edu.cn; Fax: +86-20-39943000

Authors

Yadan Huang – School of Pharmaceutical Sciences, Sun Yat-Sen University, Guangzhou 510006, P. R. China

Xu-Nian Wu – School of Pharmaceutical Sciences, Sun Yat-Sen University, Guangzhou 510006, P. R. China

Qian Zhou – School of Pharmaceutical Sciences, Sun Yat-Sen University, Guangzhou 510006, P. R. China

Yinuo Wu – School of Pharmaceutical Sciences, Sun Yat-Sen University, Guangzhou 510006, P. R. China

Dongxiao Zheng – Key Laboratory of Tropical Biological Resources of Ministry of Education, School of Life and Pharmaceutical Sciences, Hainan University, Haikou 570228, Hainan, China

Zhe Li – School of Pharmaceutical Sciences, Sun Yat-Sen University, Guangzhou 510006, P. R. China

Lei Guo – School of Pharmaceutical Sciences, Sun Yat-Sen University, Guangzhou 510006, P. R. China

Complete contact information is available at:

<https://pubs.acs.org/10.1021/acs.jmedchem.0c01573>

Author Contributions

[§]Y.H., X.-N.W., and Q.Z. contributed equally.

Notes

The authors declare no competing financial interest.

ACKNOWLEDGMENTS

This work was supported by the National Natural Science Foundation of China (21877134, 22077143, and 81903542), the Science Foundation of Guangdong Province (2020A111128007, 2014A020210009, and 2018A030313215), the Science Foundation of Guangzhou City (201904020023), and the Fundamental Research Funds for the Central Universities (no. 20ykpy112). We sincerely thank the anonymous reviewers for their constructive comments on this paper.

ABBREVIATIONS

PDE8A, phosphodiesterase 8A; IC₅₀, half-inhibitory concentration; IBMX, 3-isobutyl-1-methylxanthine; VaD, vascular dementia; cAMP, cyclic adenosine 3',5'-monophosphate; cGMP, cyclic guanosine 3',5'-monophosphate; PDEs, phosphodiesterases; FDA, Food and Drug Administration; PDB, Protein Data Bank; PAINS, pan-assay interference compounds; NBS, N-bromosuccinimide; SAR, structure–activity relationship; SD, standard deviation/Sprague-Dawley; hERG, human

ether-a-go-go-related gene; $t_{1/2}$, half-time; T_{max} , peak time; C_{max} , peak concentration; AUC, area under the curve; MRT, mean residence time; F , bioavailability; i.v., intravenous administration; p.o., oral administration; PD, pharmacodynamics; HPLC, high-performance liquid chromatography; CYP, cytochrome P450; PPB, plasma protein binding; BBB, blood–brain barrier; PAMPA, parallel artificial membrane permeation assay; CNS, central nervous system; MWM, Morris water maze; UCCAO, unilateral common carotid artery occlusion; ELT, escape latency time; SEM, standard error of the mean; TLC, thin-layer chromatography; HRMS, high-resolution mass spectrometry; EA, ethyl acetate; PE, petroleum ether; DCM, dichloromethane; DMF, *N,N*-dimethylformamide; THF, tetrahydrofuran; AIBN, 2,2'-azobis-isobutyronitrile; DMSO, dimethyl sulfoxide; IPTG, isopropyl- β -D-thiogalactopyranoside

REFERENCES

- (1) Conti, M.; Beavo, J. Biochemistry and Physiology of Cyclic Nucleotide Phosphodiesterases: Essential Components in Cyclic Nucleotide Signaling. *Annu. Rev. Biochem.* **2007**, *76*, 481–511.
- (2) Francis, S. H.; Blount, M. A.; Corbin, J. D. Mammalian Cyclic Nucleotide Phosphodiesterases: Molecular Mechanisms and Physiological Functions. *Physiol. Rev.* **2011**, *91*, 651–690.
- (3) Keravis, T.; Lugnier, C. Cyclic Nucleotide Phosphodiesterase (PDE) Isozymes as Targets of the Intracellular Signalling Network: Benefits of PDE Inhibitors in Various Diseases and Perspectives for Future Therapeutic Developments. *Br. J. Pharmacol.* **2012**, *165*, 1288–1305.
- (4) Omori, K.; Kotera, J. Overview of PDEs and Their Regulation. *Circ. Res.* **2007**, *100*, 309–327.
- (5) Pissarnitski, D. Phosphodiesterase 5 (PDE 5) Inhibitors for the Treatment of Male Erectile Disorder: Attaining Selectivity Versus PDE6. *Med. Res. Rev.* **2006**, *26*, 369–395.
- (6) Kokkonen, K.; Kass, D. A. Nanodomain Regulation of Cardiac Cyclic Nucleotide Signaling by Phosphodiesterases. *Annu. Rev. Pharmacol. Toxicol.* **2017**, *57*, 455–479.
- (7) Galie, N.; Ghofrani, H. A.; Torbicki, A.; Barst, R. J.; Rubin, L. J.; Badesch, D.; Fleming, T.; Parpia, T.; Burgess, G.; Branzi, A.; Grimminger, F.; Kurzyna, M.; Simonneau, G. Sildenafil Citrate Therapy for Pulmonary Arterial Hypertension. *N. Engl. J. Med.* **2005**, *353*, 2148–2157.
- (8) Baillie, G. S.; Tejada, G. S.; Kelly, M. P. Therapeutic Targeting of 3',5'-Cyclic Nucleotide Phosphodiesterases: Inhibition and Beyond. *Nat. Rev. Drug Discovery* **2019**, *18*, 770–796.
- (9) Kumar, A.; Singh, N. Inhibitor of Phosphodiesterase-4 Improves Memory Deficits, Oxidative Stress, Neuroinflammation and Neuro-pathological Alterations in Mouse Models of Dementia of Alzheimer's Type. *Biomed. Pharmacother.* **2017**, *88*, 698–707.
- (10) Jabaris, S. G. S. L.; Sumathy, H.; Kumar, R. S.; Narayanan, S.; Thanikachalam, S.; Babu, C. S. Effects of Rolipram and Roflumilast, Phosphodiesterase-4 Inhibitors, on Hypertension-Induced Defects in Memory Function in Rats. *Eur. J. Pharmacol.* **2015**, *746*, 138–147.
- (11) Martinez, A.; Gil, C. cAMP-Specific Phosphodiesterase Inhibitors: Promising Drugs for Inflammatory and Neurological Diseases. *Expert Opin. Ther. Pat.* **2014**, *24*, 1311–1321.
- (12) Rutten, K.; Basile, J. L.; Prickaerts, J.; Blokland, A.; Vivian, J. A. Selective PDE Inhibitors Rolipram and Sildenafil Improve Object Retrieval Performance in Adult Cynomolgus Macaques. *Psychopharmacology* **2008**, *196*, 643–648.
- (13) Monti, B.; Berteotti, C.; Contestabile, A. Subchronic Rolipram Delivery Activates Hippocampal CREB and Arc, Enhances Retention and Slows down Extinction of Conditioned Fear. *Neuropsychopharmacology* **2006**, *31*, 278–286.
- (14) Guo, H.; Cheng, Y.; Wang, C.; Wu, J.; Zou, Z.; Niu, B.; Yu, H.; Wang, H.; Xu, J. FFPM, a PDE4 Inhibitor, Reverses Learning and Memory Deficits in APP/PS1 Transgenic Mice via cAMP/PKA/

CREB Signaling and anti-Inflammatory Effects. *Neuropharmacology* **2017**, *116*, 260–269.

(15) Liang, J.; Huang, Y.-Y.; Zhou, Q.; Gao, Y.; Li, Z.; Wu, D.; Yu, S.; Guo, L.; Chen, Z.; Huang, L.; Liang, S. H.; He, X.; Wu, R.; Luo, H.-B. Discovery and Optimization of α -Mangostin Derivatives as Novel PDE4 Inhibitors for the Treatment of Vascular Dementia. *J. Med. Chem.* **2020**, *63*, 3370–3380.

(16) Boswell-Smith, V.; Spina, D.; Page, C. P. Phosphodiesterase Inhibitors. *Br. J. Pharmacol.* **2006**, *147*, S252–S257.

(17) Vercambre, M.-N.; Berr, C.; Ritchie, K.; Kang, J. H. Caffeine and Cognitive Decline in Elderly Women at High Vascular Risk. *J. Alzheimer's Dis.* **2013**, *35*, 413–421.

(18) Driscoll, I.; Shumaker, S. A.; Snively, B. M.; Margolis, K. L.; Manson, J. E.; Vitolins, M. Z.; Rossom, R. C.; Espeland, M. A. Relationships Between Caffeine Intake and Risk for Probable Dementia or Global Cognitive Impairment: The Women's Health Initiative Memory Study. *J. Gerontol., Ser. A* **2016**, *71*, 1596–1602.

(19) Tsai, L.-C. L.; Chan, G. C.-K.; Nangle, S. N.; Shimizu-Albergine, M.; Jones, G. L.; Storm, D. R.; Beavo, J. A.; Zweifel, L. S. Inactivation of Pde8b Enhances Memory, Motor Performance, and Protects against Age-Induced Motor Coordination Decay. *Genes, Brain Behav.* **2012**, *11*, 837–847.

(20) Wang, P.; Myers, J. G.; Wu, P.; Cheewatrakoolpong, B.; Egan, R. W.; Billah, M. M. Expression, Purification, and Characterization of Human cAMP-Specific Phosphodiesterase (PDE4) Subtypes A, B, C, and D. *Biochem. Biophys. Res. Commun.* **1997**, *234*, 320–324.

(21) Soderling, S. H.; Bayuga, S. J.; Beavo, J. A. Cloning and Characterization of a cAMP-Specific Cyclic Nucleotide Phosphodiesterase. *Proc. Natl. Acad. Sci. U.S.A.* **1998**, *95*, 8991–8996.

(22) Gamanuma, M.; Yuasa, K.; Sasaki, T.; Sakurai, N.; Kotera, J.; Omori, K. Comparison of Enzymatic Characterization and Gene Organization of Cyclic Nucleotide Phosphodiesterase 8 Family in Humans. *Cell. Signalling* **2003**, *15*, 565–574.

(23) Fisher, D. A.; Smith, J. F.; Pillar, J. S.; St. Denis, S. H.; Cheng, J. B. Isolation and Characterization of PDE8A, a Novel Human cAMP-Specific Phosphodiesterase. *Biochem. Biophys. Res. Commun.* **1998**, *246*, 570–577.

(24) Snyder, H. M.; Corriveau, R. A.; Craft, S.; Faber, J. E.; Greenberg, S. M.; Knopman, D.; Lamb, B. T.; Montine, T. J.; Nedergaard, M.; Schaffer, C. B.; Schneider, J. A.; Wellington, C.; Wilcock, D. M.; Zipfel, G. J.; Zlokovic, B.; Bain, L. J.; Bosetti, F.; Galis, Z. S.; Koroshetz, W.; Carrillo, M. C. Vascular Contributions to Cognitive Impairment and Dementia Including Alzheimer's Disease. *Alzheimer's Dementia* **2015**, *11*, 710–717.

(25) Demirbas, D.; Wyman, A. R.; Shimizu-Albergine, M.; Cakici, O.; Beavo, J. A.; Hoffman, C. S. A Yeast-Based Chemical Screen Identifies a PDE Inhibitor that Elevates Steroidogenesis in Mouse Leydig Cells via PDE8 and PDE4 Inhibition. *PLoS One* **2013**, *8*, No. e71279.

(26) DeNinno, M. P.; Wright, S. W.; Visser, M. S.; Etienne, J. B.; Moore, D. E.; Olson, T. V.; Rocke, B. N.; Andrews, M. P.; Zarbo, C.; Millham, M. L.; Boscoe, B. P.; Boyer, D. D.; Doran, S. D.; Houseknecht, K. L. 1,5-Substituted Nipicotic Amides: Selective PDE8 Inhibitors Displaying Diastereomer-Dependent Microsomal Stability. *Bioorg. Med. Chem. Lett.* **2011**, *21*, 3095–3098.

(27) DeNinno, M. P.; Wright, S. W.; Etienne, J. B.; Olson, T. V.; Rocke, B. N.; Corbett, J. W.; Kung, D. W.; DiRico, K. J.; Andrews, K. M.; Millham, M. L.; Parker, J. C.; Esler, W.; van Volkenburg, M.; Boyer, D. D.; Houseknecht, K. L.; Doran, S. D. Discovery of Triazolopyrimidine-Based PDE8B Inhibitors: Exceptionally Ligand-Efficient and Lipophilic Ligand-Efficient Compounds for the Treatment of Diabetes. *Bioorg. Med. Chem. Lett.* **2012**, *22*, 5721–5726.

(28) Fisher, D. A.; Smith, J. F.; Pillar, J. S.; St. Denis, S. H.; Cheng, J. B. Isolation and Characterization of PDE9A, a Novel Human cGMP-Specific Phosphodiesterase. *J. Biol. Chem.* **1998**, *273*, 15559–15564.

(29) Meng, F.; Hou, J.; Shao, Y.-X.; Wu, P.-Y.; Huang, M.; Zhu, X.; Cai, Y.; Li, Z.; Xu, J.; Liu, P.; Luo, H.-B.; Wan, Y.; Ke, H. Structure-Based Discovery of Highly Selective Phosphodiesterase-9A Inhibitors

and Implications for Inhibitor Design. *J. Med. Chem.* **2012**, *55*, 8549–8558.

(30) Shao, Y.-x.; Huang, M.; Cui, W.; Feng, L.-J.; Wu, Y.; Cai, Y.; Li, Z.; Zhu, X.; Liu, P.; Wan, Y.; Ke, H.; Luo, H.-B. Discovery of a Phosphodiesterase 9A Inhibitor as a Potential Hypoglycemic Agent. *J. Med. Chem.* **2014**, *57*, 10304–10313.

(31) Qiu, X.; Huang, Y.; Wu, D.; Mao, F.; Zhu, J.; Yan, W.; Luo, H.-B.; Li, J. Discovery of Novel Purine Nucleoside Derivatives as Phosphodiesterase 2 (PDE2) inhibitors: Structure-Based Virtual Screening, Optimization and Biological Evaluation. *Bioorg. Med. Chem.* **2018**, *26*, 119–133.

(32) Baell, J. B.; Holloway, G. A. New Substructure Filters for Removal of Pan Assay Interference Compounds (PAINS) from Screening Libraries and for their Exclusion in Bioassays. *J. Med. Chem.* **2010**, *53*, 2719–2740.

(33) Miyaura, N.; Suzuki, A. Palladium-Catalyzed Cross-Coupling Reactions of Organoboron Compounds. *Chem. Rev.* **1995**, *95*, 2457–2483.

(34) Wohl, A. Bromierung ungesättigter Verbindungen mit N-Bromacetamid, ein Beitrag zur Lehre vom Verlauf chemischer Vorgänge. *Ber. Dtsch. Chem. Ges.* **1919**, *52*, 51–63.

(35) Ziegler, K.; Schenck, G.; Krockow, E. W.; Siebert, A.; Wenz, A.; Weber, H. Die Synthese des Cantharidins. *Justus Liebig's Ann. Chem.* **1942**, *551*, 1–79.

(36) Wang, H.; Yan, Z.; Yang, S.; Cai, J.; Robinson, H.; Ke, H. Kinetic and Structural Studies of Phosphodiesterase-8A and Implication on the Inhibitor Selectivity. *Biochemistry* **2008**, *47*, 12760–12768.

(37) Di, L.; Kerns, E. H.; Fan, K.; McConnell, O. J.; Carter, G. T. High Throughput Artificial Membrane Permeability Assay for Blood-Brain Barrier. *Eur. J. Med. Chem.* **2003**, *38*, 223–232.

(38) Farooq, M. U.; Min, J.; Goshgarian, C.; Gorelick, P. B. Pharmacotherapy for Vascular Cognitive Impairment. *CNS Drugs* **2017**, *31*, 759–776.

(39) Bhatia, P.; Singh, N. Tadalafil Ameliorates Memory Deficits, Oxidative Stress, Endothelial Dysfunction and Neuropathological Changes in Rat Model of Hyperhomocysteinemia Induced Vascular Dementia. *Int. J. Neurosci.* **2020**, 1–13.

(40) Jian, W.-X.; Zhang, Z.; Zhan, J.-H.; Chu, S.-F.; Peng, Y.; Zhao, M.; Wang, Q.; Chen, N.-H. Donepezil Attenuates Vascular Dementia in Rats through Increasing BDNF Induced by Reducing HDAC6 Nuclear Translocation. *Acta Pharmacol. Sin.* **2020**, *41*, 588–598.

(41) Sun, Y.; Zhao, Z.; Li, Q.; Wang, C.; Ge, X.; Wang, X.; Wang, G.; Qin, Y. DL-3-n-Butylphthalide Regulates Cholinergic Dysfunction in Chronic Cerebral Hypoperfusion Rats. *J. Int. Med. Res.* **2020**, *48*, 0300060520936177.

(42) Jain, A. N. Surflex: Fully Automatic Flexible Molecular Docking Using a Molecular Similarity-Based Search Engine. *J. Med. Chem.* **2003**, *46*, 499–511.

(43) Yan, Z.; Wang, H.; Cai, J.; Ke, H. Refolding and Kinetic Characterization of the Phosphodiesterase-8A Catalytic Domain. *Protein Expression Purif.* **2009**, *64*, 82–88.

(44) Li, Z.; Cai, Y.-H.; Cheng, Y.-K.; Lu, X.; Shao, Y.-X.; Li, X.; Liu, M.; Liu, P.; Luo, H.-B. Identification of Novel Phosphodiesterase-4D Inhibitors Prescreened by Molecular Dynamics-Augmented Modeling and Validated by Bioassay. *J. Chem. Inf. Model.* **2013**, *53*, 972–981.

(45) Wu, D.; Huang, Y.; Chen, Y.; Huang, Y.-Y.; Geng, H.; Zhang, T.; Zhang, C.; Li, Z.; Guo, L.; Chen, J.; Luo, H.-B. Optimization of Chromeno[2,3-c]pyrrol-9(2H)-ones as Highly Potent, Selective, and Orally Bioavailable PDE5 Inhibitors: Structure–Activity Relationship, X-ray Crystal Structure, and Pharmacodynamic Effect on Pulmonary Arterial Hypertension. *J. Med. Chem.* **2018**, *61*, 8468–8473.

(46) Wang, H.; Liu, Y.; Chen, Y.; Robinson, H.; Ke, H. Multiple Elements Jointly Determine Inhibitor Selectivity of Cyclic Nucleotide Phosphodiesterases 4 and 7. *J. Biol. Chem.* **2005**, *280*, 30949–30955.

(47) Park, S.-J.; Ahmad, F.; Philp, A.; Baar, K. Resveratrol Ameliorates Aging-Related Metabolic Phenotypes by Inhibiting cAMP Phosphodiesterases. *Cell* **2012**, *148*, 421–433.

(48) Wu, D.; Zhang, T.; Chen, Y.; Huang, Y.; Geng, H.; Yu, Y.; Zhang, C.; Lai, Z.; Wu, Y.; Guo, X.; Chen, J.; Luo, H.-B. Discovery and Optimization of Chromeno[2,3-c]pyrrol-9(2H)-ones as Novel Selective and Orally Bioavailable Phosphodiesterase 5 Inhibitors for the Treatment of Pulmonary Arterial Hypertension. *J. Med. Chem.* **2017**, *60*, 6622–6637.

(49) Huang, Y.-Y.; Yu, Y.-F.; Zhang, C.; Chen, Y.; Zhou, Q.; Li, Z.; Zhou, S.; Li, Z.; Guo, L.; Wu, D.; Wu, Y.; Luo, H.-B. Validation of Phosphodiesterase-10 as a Novel Target for Pulmonary Arterial Hypertension via Highly Selective and Subnanomolar Inhibitors. *J. Med. Chem.* **2019**, *62*, 3707–3721.

(50) Yang, Y.; Zhang, S.; Zhou, Q.; Zhang, C.; Gao, Y.; Wang, H.; Li, Z.; Wu, D.; Wu, Y.; Huang, Y.-Y.; Guo, L.; Luo, H.-B. Discovery of Highly Selective and Orally Available Benzimidazole-Based Phosphodiesterase 10 Inhibitors with Improved Solubility and Pharmacokinetic Properties for Treatment of Pulmonary Arterial Hypertension. *Acta Pharm. Sin. B* **2020**, DOI: [10.1016/j.apsb.2020.04.003](https://doi.org/10.1016/j.apsb.2020.04.003).

(51) Wu, Y.; Zhou, Q.; Zhang, T.; Li, Z.; Chen, Y.-P.; Zhang, P.; Yu, Y.-F.; Geng, H.; Tian, Y.-J.; Zhang, C.; Wang, Y.; Chen, J.-W.; Chen, Y.; Luo, H.-B. Discovery of Potent, Selective, and Orally Bioavailable Inhibitors against Phosphodiesterase-9, a Novel Target for the Treatment of Vascular Dementia. *J. Med. Chem.* **2019**, *62*, 4218–4224.

(52) Lu, C.; Guo, Y.; Yan, J.; Luo, Z.; Luo, H.-B.; Yan, M.; Huang, L.; Li, X. Design, Synthesis, and Evaluation of Multitarget-Directed Resveratrol Derivatives for the Treatment of Alzheimer's Disease. *J. Med. Chem.* **2013**, *56*, 5843–5859.